Effect of hot pressing method on utilization of catalyst in PEMFC electrodes fabricated via electrospray

_____

Christian Ayuste

APPROVED:

_____

Dr. Anima Bose, Associate Professor
Committee Chair
Engineering Technology

_____

Dr. Jian Shi, Assistant Professor
Engineering Technology

_____

Dr. Zheng Fan, Assistant Professor
Engineering Technology

_____

Dr. Wajiha Shireen, Department Chair
Engineering Technology

_____

Dr. George Zouridakis, Associate Dean
College of Technology

Effect of hot pressing on utilization of catalyst in PEMFC electrodes fabricated via electrospray

By

Christian Ayuste

A thesis presented in fulfillment of the requirements for the degree of

Master of Science

in Material and Mechanical in the

Department of Engineering Technology

College of Technology

University of Houston

2018

Houston, Texas

Abstract

A lab-scale electrospraying system has been designed and spray parameters were optimized for the fabrication of electrodes with consistent and uniform catalyst loading for Proton Exchange Membrane Fuel Cell (PEMFC) applications. In order to understand the effect of electrodes designed through the electrospraying technique in PEMFC's, a series of membrane-electrode assemblies (MEA's) were prepared by varying the MEA fabrication hot-pressing parameters of pressure, temperature, and time. The evaluated performance of MEA's were varied primarily due to differences in hot pressing condition of MEA fabrication, and due to cell operating conditions. At 80°C and 100% relative humidity operating conditions, an MEA hot-pressed at 8 MPa for 390 seconds at a temperature of 150°C generated peak power density of 903 mW/cm^2, current density of 1040 mA/cm^2 at 0.6V, had a Tafel slope of 95.64 mV/dec, and electrochemical surface area (ECSA) of 23.96 m^2/g$_{Pt}$. On the other hand, an MEA hot-pressed for the same length of time at the same temperature but with a lower pressure of 2.67 MPa generated higher peak power density of 1130 mW/cm^2, higher current density of 1040 mA/cm^2 at 0.6V, and had a Tafel slope of 90.07 mV/dec despite having a lower ECSA of 19.18 m^2/g$_{Pt}$. Overall, results of this study support a low hot-pressing pressure as well as a high pressing temperature for producing the highest achievable performance from electrosprayed electrodes.

Contents

Table of Figures

List of Tables

Chapter 1: Introduction and Literature Review

1.0 Introduction

The internal combustion engine (ICE) is currently the most common form of power-generation used for vehicle transportation across the globe. However, with increased public concerns regarding carbon emissions [1] as well as advancements in renewable energy technologies, automakers are increasingly providing vehicle options which are powered either partially or solely with electricity [2]. One option for electric vehicle power which is under development by several automakers is the Polymer Electrolyte Membrane Fuel Cell (PEMFC). Major automakers Toyota and Honda have already released their Mirai and Clarity models, respectively, as the first few Fuel Cell Vehicles (FCVs) available to consumers [3].

Though there are several types of fuel cells available, PEMFCs are seen as the best option for consumer vehicles for the following reasons: 1) low operating temperature [4], 2) relatively quick start-up [5], and 3) high power density [6]. However, increased commercialization of PEMFCs for applications such as vehicle transportation requires reductions in both the cost of manufacturing and cost of operation as well as increased performance from the fuel cell. One of the most expensive portions of PEMFC manufacturing lies in the cost of the material, specifically the electrodes and the catalyst within the electrodes, which are crucial to operation. The catalyst has been estimated to account for more than 50% of the cost of a fuel cell [7], and, thus, fuel cell electrode development and fabrication center around the reduction of catalyst used in a fuel cell, which is known as the "catalyst loading".

Several fabrication methods have been developed to produce suitable fuel cell electrodes, examples are: brushing [8], decal method [9], screen-printing method [10], and electrostatic spray (typically referred to as "electrospray"). Of these methods, electrospray has been shown to produce electrodes with high catalyst utilization compared to others [11][12], which consequently results in lower catalyst loadings but similar performance as electrodes with higher catalyst loadings.

In this work, an electrode fabrication system using electrospray was developed to produce high performance electrodes with low catalyst loadings and the effects of the hot-pressing manufacturing step on electrodes produced via electrospray were studied. These topics were studied since previous works have not provided much detail regarding how the various manufacturing steps of electrosprayed MEAs (such as spraying parameters, ink composition, and hot pressing parameters) affect the final performance of said MEAs.

1.1 Fuel Cell Basics

In addition to the Polymer Electrolyte Membrane Fuel Cell (PEMFC), there are several other types such as the Direct Methanol Fuel Cell (DMFC), Alkaline Fuel Cell, Solid Oxide Fuel Cell (SOFC), etc. Each of the fuel cell types is classified by the type of electrolyte employed and each is better suited for specific applications [13]. For example, due to its low operating temperature and high efficiency, the PEMFC is well-suited for portable applications such as mobile phone charging in addition to vehicle power applications mentioned previously. Though each fuel cell type is better suited for different applications, all fuel cells operate based on a similar principle and have the

same basic components. These components are: bipolar plates, current collectors, gas diffusion layers, and a membrane electrode assembly (MEA) which consists of an electrolyte membrane with electrodes on both sides. These components will be described in detail in following sections.

1.2 Fuel Cell Operation

All fuel cells operate in the following manner: 1) fuel is fed to either the anode or cathode while an oxidant is fed to the other electrode, 2) a chemical reaction occurs on the fuel-side electrode which removes electrons from the fuel, 3) the electrons move through the fuel-side current collector and eventually arrive at the oxidant-side electrode through the oxidant-side current collector, 4) while the electrons are moving through the current collectors (generating electricity), the ions created from the fuel-side reaction pass through the electrolyte medium and arrive at the oxidant-side electrode, 5) the ions from the fuel-side reaction interact with the oxidant on the oxidant-side electrode and the product is expelled.

In the case of the PEMFC, the fuel is typically pure hydrogen gas (H_2) which is fed into the anode side of the fuel cell, and the oxidant can be either pure oxygen gas (O_2) or air which is fed to the cathode side of the fuel cell. The reaction (RXN) which occurs on the anode-side creates positive Hydrogen ions and electrons. The Hydrogen ions pass through the electrolyte membrane while the electrons are forced to travel through the current collector plate. The electrons travel through the anode-side current collector plate and arrive at the cathode via the cathode-side current collector plate. The Hydrogen ions, electrons, and Oxygen (either in pure gas form or from air) react on the

cathode-side to generate water (H_2O) and heat. Reference the diagram in Figure 1 for a visual representation of the process. Each of the components in Figure 1 will be explained in more detail in following sections.

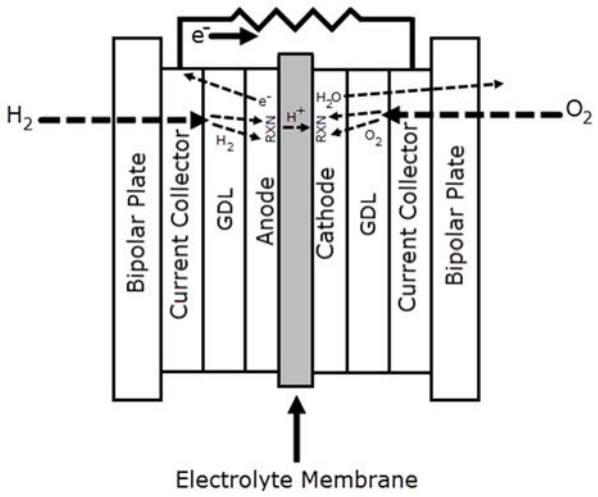

Figure 1: Visual representation of PEMFC reaction process

1.2.1 Bipolar Plates

The bipolar plates of the fuel cell serve as the structure which contains and binds the components mentioned previously, while simultaneously acting as a pipeline for reactants and products which flow through the Gas Diffusion Layer (GDL) to and from the electrodes. The bipolar plates are typically designed with channels known as "flow fields" which face the GDL's of the fuel cell. Reactants flow into the bipolar plates, through the channels, diffuse through the GDL, and then reach the electrodes to feed the electrochemical reactions of the fuel cell. The bipolar plates then also allow products such as water to exit the fuel cell. Reference Figure 2 on the next page for a depiction of flow of reactants through the bipolar plates.

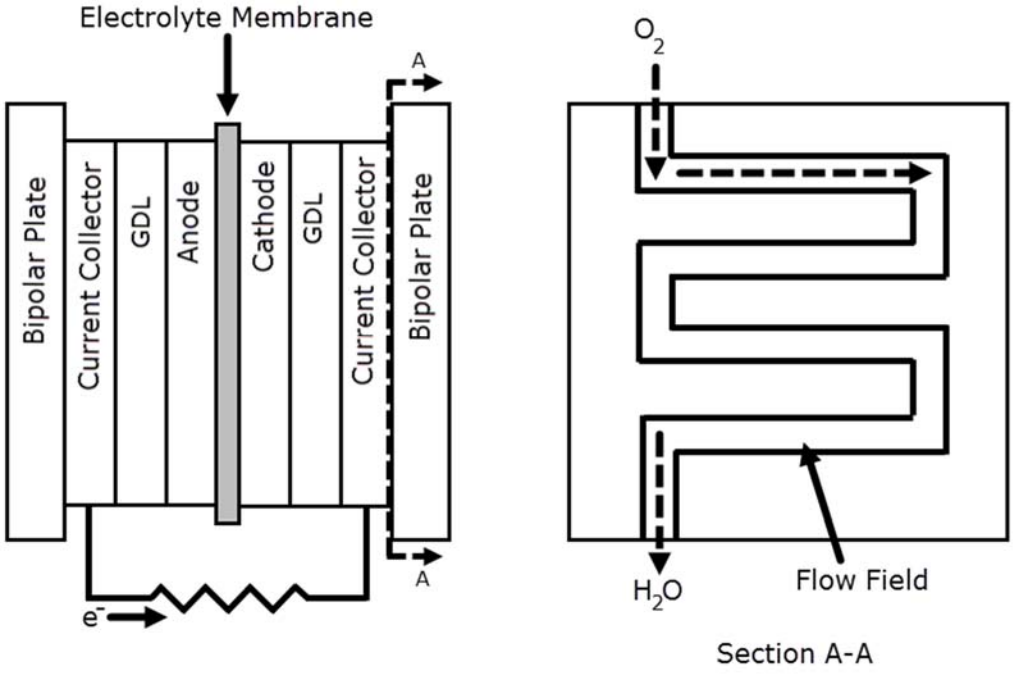

Figure 2: Bipolar plate positions in a PEMFC and flow of fuel cell reactants through bipolar plates (Section A-A)

1.2.2 Current Collector Plates

The current collector plates are located on both the anode and cathode sides of the fuel cell, and they allow the flow of electrons from one side of the fuel cell to the other. For a PEMFC, the current collector plate on the anode side “collects” the electrons which are obtained from the hydrogen reaction, and then the electrons are transferred through the collector plate, through some load (such as a light bulb as mentioned previously), and then to the cathode side collector plate.

1.2.3 Gas Diffusion Layers

The Gas Diffusion Layer (GDL) allows gases which fuel the chemical reactions to be delivered to the electrodes in a uniform and consistent manner. In the case of the

PEMFC, the gas diffusion layer is typically very porous and made from either carbon cloth or carbon paper. The porosity of the GDL is a significant factor to the operation of the fuel cell since porosity not only allows gases to the electrodes but also allows products from the chemical reactions to be carried away from the electrodes.

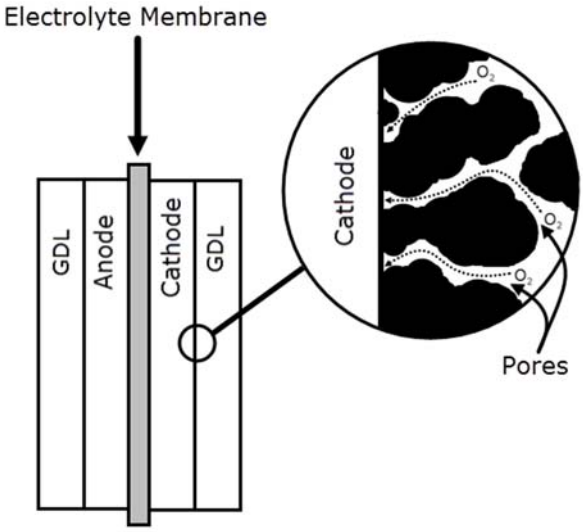

Figure 3: GDL position in a PEMFC and example flow through pore structure.

1.2.4 Electrolyte Membrane

The electrolyte membrane is typically described along with the fuel cell electrodes as the Membrane Electrode Assembly (MEA) since these components operate hand-in-hand. In the case of the PEMFC, hydrogen ions conduct from the anode side of the membrane, through the polymer electrolyte membrane, and then react with oxygen on the cathode side of the membrane. Since the electrons from the anode side cannot travel through the electrolyte, the electrons must travel around it by conducting through the current collector.

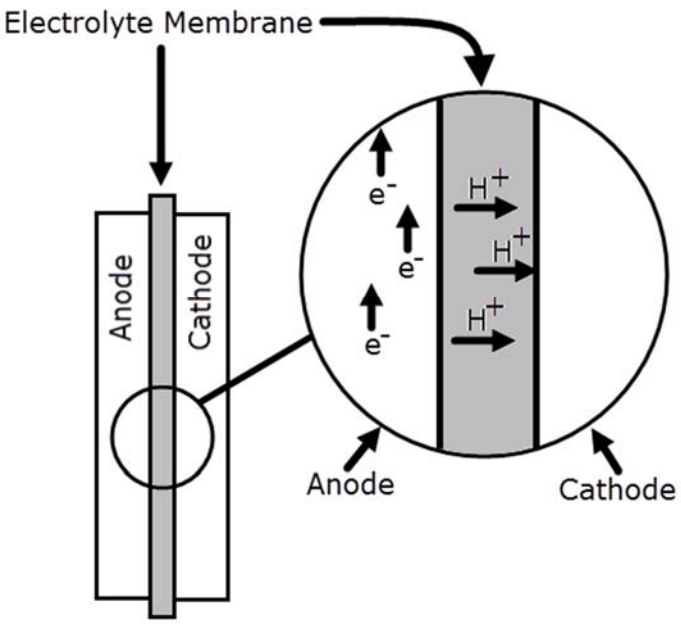

Figure 4: Membrane allowing flow of H^+ ions while preventing flow of electrons.

1.2.5 Electrodes

The electrodes of a fuel cell provide the locations at which the necessary chemical reactions occur to generate ions and counterions. For a PEMFC, the electrodes (both the anode and the cathode) contain catalyst particles which initiate the chemical reactions. Ideally, these catalyst particles are in contact with channels made of the same electrolyte as the membrane, while also simultaneously in contact with carbon particles which are also present in the electrode. The electrolyte channel and the carbon particles allow the ions and counterions from the reaction which occur at the catalyst to be carried away through either the electrolyte membrane or the current collector plates. The point at which the catalyst, carbon, and electrolyte interface is known as a three-phase or triple-phase boundary, and the presence of more three-phase boundaries increases the performance of the electrode and subsequently the fuel cell.

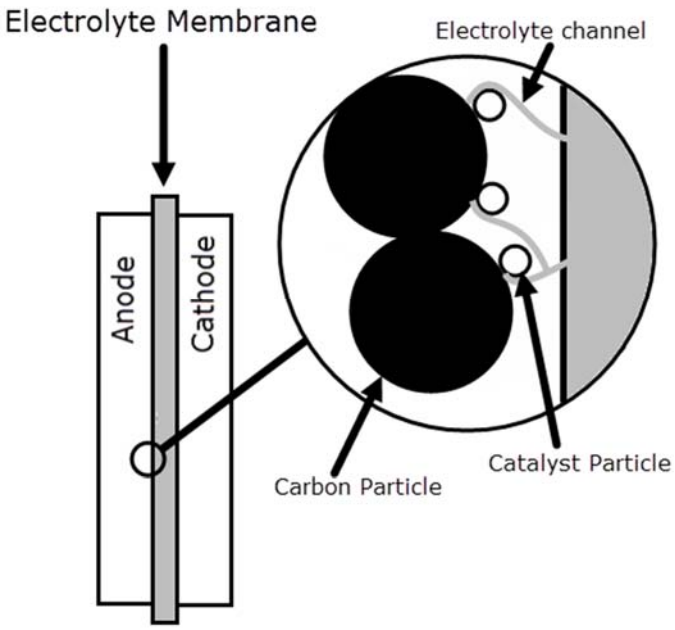

Figure 5: Representation of three-phase boundary in a PEMFC

1.2.5.1 Electrode Fabrication Methods

Electrodes are critical components in fuel cells due to the central role they play in the necessary chemical reactions; therefore, they must be durable as well as high-performing. In addition, fuel cell electrodes must also have: low catalyst loadings, high catalyst utilization [14], high electronic conductivity, mechanical stability, and adequate porosity [15]. Several electrode fabrication methods have been developed over time, and each results in varying pros and cons to certain electrode characteristics; however, this section only covers a few of the most common lab-scale methods as well as the electrospray method.

1.2.5.2 Decal/Thin-Film Method

The decal (or “thin-film”) method was first introduced by Wilson and Gottesfeld in 1992 [9] The schematic representation of the various steps involved in decal method is provided in Figure 6. The decal method begins with a catalyst ink specifically formulated to be relatively viscous. The viscosity of the ink is achieved with the use of glycerol and water, and it is an important factor for holding the carbon particles within the ink in suspension while also preventing their agglomeration. Additionally, the viscosity also allows the ink to be easily applied to a Teflon blank (a) which will be used to transfer the ink to the electrolyte membrane at a later step.

Once the catalyst ink is prepared, it is applied to the Teflon blank (b) and the Teflon blank with the catalyst ink applied to its surface is baked (c). Additional layers can be added by repeating the ink application and baking processes until the desired catalyst loading is achieved. After baking the catalyst ink onto the Teflon blank, the catalyst layer is then applied to the electrolyte membrane by pressing the two together (d) with a large amount of pressure as well as high heat (a process known as “hot pressing”). Typically, both the anode and cathode are hot-pressed to the electrolyte membrane simultaneously. The result is an MEA which consists of a polymer electrolyte membrane with the anode and cathode attached on either side (e).

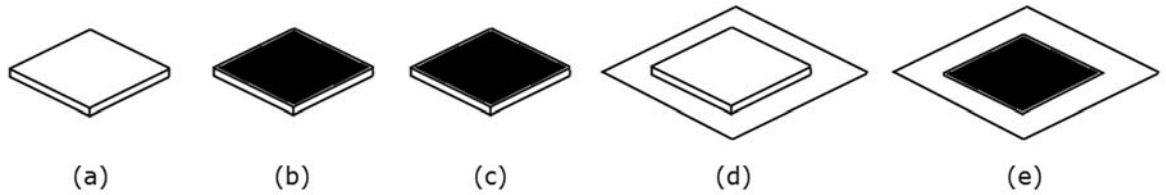

Figure 6: Decal method preparation and application

Wilson and Gottesfeld made only the cathodes of their MEA's using the decal method, citing the reduction reaction on the cathode as the most challenging for the catalyst layer when compared to the oxidation reaction on the anode. The cathodes produced were made with 19.8 wt% Platinum-on-Carbon (Pt/C) catalyst. The cathode catalyst loadings studied were 0.20 and 0.35 mg/cm^2 .

In their work, Wilson and Gottesfeld report that the thickness of the catalyst layer has a significant effect on the current density and subsequently the cell voltage. When a thicker cathode catalyst layer is operated, the cell voltages are higher than those obtained from slightly thinner cathode catalyst layers. However, as the current densities increase, the thinner cathodes are shown to achieve higher cell voltages. According to Wilson and Gottesfeld, this is due to less of the catalyst layer being utilized and the increased significance of mass transfer effects at higher densities.

In 1999, Cheng et al. [16] evaluated the platinum utilization of the thin-film catalyst layer produced by Wilson and Gottesfeld's decal method. They calculated the platinum utilization to be 45.4%. Cheng et al. attributed the extremely low utilization to the presence of Nafion and its blocking of electron pathways in the catalyst layer. For comparison, they impregnated an E-TEK brand commercial gas-diffusion electrode with Nafion by immersing the electrode in a solution of 2.5 wt% Nafion. From the impregnated E-TEK electrode, a platinum utilization of 77.8% was calculated, which was attributed to the fact that the electron conduction pathways were already fixed and

could not be affected by the addition of Nafion. Instead, the addition of Nafion via immersion, simply increased the number of proton conduction pathways.

Xie et al. further developed the decal method in 2004 by studying the effects of the transfer decal, the catalyst layer application process, and the lubricant between the decal and the catalyst layer [17]. They discovered that the multi-layer brush painting in combination with the use of Teflon as the transfer medium first used by Wilson and Gottesfeld creates a skin of proton-conducting ionomer at the interface between the catalyst layer and the Teflon transfer medium. Once the catalyst layer is hot-pressed to the electrolyte membrane, the ionomer skin then faces the gas diffusion layer when installed into the fuel cell. Since the ionomer skin is hydrophobic, its location between the gas diffusion layer and catalyst layer restricts the escape of water which is produced during operation of the fuel cell, which causes flooding. Xie et al. modified Wilson and Gottesfeld's original decal method by using a far-less-hydrophobic transfer medium, Kapton, instead of the original Teflon. Furthermore, Xie et al. used a blade coating process to achieve the desired catalyst loading in one layer rather than using multiple brushed layers.

Up until 2006, the decal/thin-film method and its many variations composed the bulk of the state of the art in PEMFC technology. However, this method had several limitations such as uniformity of deposition when applied to large-scale manufacturing and also high cost due to the complex processes and/or the number of steps necessary [18]. Furthermore, though recent works continue to improve the decal method, catalyst loadings to achieve acceptable performance are still relatively high compared to more modern methods employed in PEMFC electrodes fabrication. For example, a 2018

study using the decal method had loadings of 0.4 mg/cm^2 [19] and a 2017 study required 0.5 mg/cm^2 [20].

1.2.5.3 Screen-Printing Method

The screen-printing method was first introduced in 1998 by Kim et al in order to provide a cost-effective PEMFC MEA preparation method which was also capable of achieving effective three-phase boundaries [10]. In their work, Kim et al. began the process by first hot-pressing a perfluorosulfonyl fluoride copolymer resin powder in a stainless steel frame and creating the base on which the catalyst ink will later be applied. Since the base is made of perfluorosulfonyl fluoride, no Nafion is added and the catalyst ink only consists of 20 wt% Pt/C, glycerol, and water. After application of the ink to perfluorosulfonyl fluoride base, the base is then hot-pressed to the electrolyte membrane (similar to the decal method mentioned previously), and then the MEA is converted into an acid type ion-exchange membrane by hydrolysis. Catalyst loading for screen-printed electrodes were reported to be 0.2 mg/cm^2. The various steps involved in the screen-printing process of electrode preparation is provided in Figure 7.

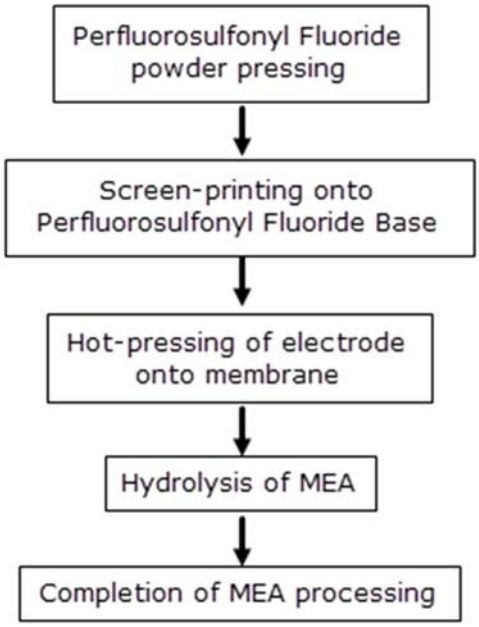

Figure 7: Flowchart of Screen-printing Process by Kim et al.

Also in 1998, Kim et al. compared the “thin-film” screen-printing MEA fabrication process to the “conventional” MEA fabrication process to determine which generated better performance [21]. In the conventional fabrication process presented, the catalyst layer is applied as slurry to the carbon paper/cloth which made up the gas diffusion layers. After application of the catalyst, the electrodes were then hot-pressed to the membrane to create MEA’s. For the thin-film method, the catalyst ink was coated directly onto the membrane via screen-printing. Afterward, carbon cloth gas diffusion layers are hot-pressed to the MEA. Comparison of single-cell testing between the conventional and thin-film methods showed that the thin-film method out-performed the conventional method by 86% more power density.

In 2003, Bender et al. further developed the screen-printing process and compared the results to the hand painting method [22]. In their work, Bender et al. uses a doctor blade spreader (aka screen printer) but the tool required a non-conventional ink formulation in order for the ink to be properly spread by the tool. The non-conventional ink was obtained by evaporating the solvents out of the conventional ink formulation and also experimenting with combinations of other solvents such as diglyme, glycerol, and water. Ultimately, the screen-printed MEA was made with non-conventional ink, and the hand-painted (aka decal method) MEA was made with conventional ink. The MEA's were then tested and Bender et al. determined that the MEA's using the non-conventional ink applied via the doctor blade spread performed better than the MEA using conventional ink applied via hand-painting. Additionally, the total application time to achieve similar loading was 87.5% faster when using the doctor blade method versus the hand-painting method (45 mins vs 6 hours).

1.2.5.4 Electrospray Method

In general, the electrospray method is used to atomize a liquid exiting from a nozzle to produce a spray of very fine droplets. This method is commonly used to coat a target substrate with a thin layer of the liquid. Electrospray requires the nozzle (typically a needle) to be kept at a very high voltage relative to the target. The high voltage of the needle generates a shear stress in the liquid exiting the needle [23], and the liquid forms a cone - known as a "Taylor Cone" - at the end of the needle. The finely atomized liquid droplets are emitted from this cone. The Taylor Cone was first examinedby John Zeleny in 1916 as he studied the effects of electricity on electrified liquids exiting a 0.92 mm

diameter glass tube. He noted that at varying levels of applied voltage and reservoir heights (aka head pressure), the liquid exiting the glass tube exhibited varying forms [24].

One of these forms was ultimately studied by Geoffrey Taylor, and in 1964, he published his first work on what would eventually be known as the Taylor Cone. The Taylor Cone was characterized by Taylor himself as a “conical interface between two fluids... in equilibrium in an electric field” with a semi-vertical angle 49.3 degrees. Furthermore, this conical interface was shown to produce a consistent axial jet of ejecting fluid [25]. Taylor studied the jet(s) further and determined that fluids at varying voltages could create an axial jet with either a long, consistent “string” of fluid or a spray of fine fluid particles [26]. These forms (as well as several other newly discovered forms) would later be classified by Cloupeau and Prunet-Foch as: dripping mode, microdripping mode, spindle mode, cone-jet mode, and multi-jet mode. [27]

Though the different modes of electrospray/electrohydrodynamic spray have their uses in varying applications, the most commonly used form is the cone-jet mode, and it is used to produce coatings in industries such as agriculture [28], automotive painting [29], inkjet printing [30], etc.

1.2.5.5 Electrospray Setup and Parameters

Typical electrospray equipment setups used for lab purposes have the following components: a nozzle (usually a needle attached to a syringe), a pump or some other method to flow liquid through the needle (usually a syringe pump), a high voltage power

supply to produce the Taylor Cone, and a collector plate, where the target to be coated is placed.

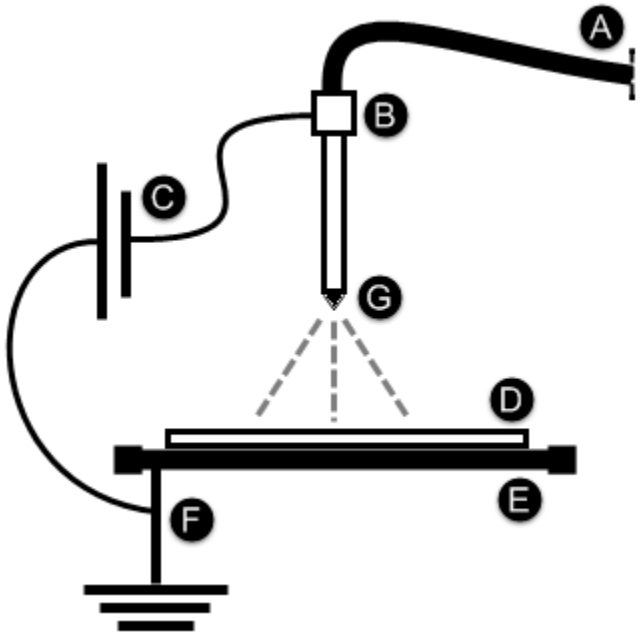

Figure 8: Diagram of a typical electrospray equipment setup. A) Feed tube from a syringe pump, B) needle, C) high voltage power supply, D) target to be coated, E) collector plate, F) ground attached to both C and E, G) Taylor Cone exiting needle.

The electrospray method is controlled by several parameters related to the aforementioned equipment and their interactions as well as interactions with the liquid being sprayed. For instance, the conductivity of the liquid being sprayed, flowrate of said liquid through the needle, and the voltage at the needle together determine whether a Taylor Cone in cone-jet mode or other spray modes are produced [27]. Additionally, the size of the droplets which are formed by the Taylor Cone can also be controlled by adjusting the flowrate and/or voltage [31]. The distance of the needle to the collector plate also has an effect on the Taylor Cone in that variations of distance change the minimum voltage to produce a Taylor Cone [32]. The needle distance and

the droplet size are critical to the resultant coating since both have an effect on how wet or dry the droplets are when they land on the target [33].

1.2.5.6 Electrode Fabrication by Electrospray

The first documented application of the electrospray process to fuel cell MEA manufacturing was written by Baturina and Wnek in 2005. In their work, Baturina and Wnek electrosprayed a Pt-based ink at a voltage of 20 KV, resulting in MEA's with catalyst loading as low as 0.09 mg/cm^2 though MEA's with loading of 0.36 mg/cm^2 were tested as well. The performance of said MEAs were reported as producing ~100 mA/cm^2 at 0.8V with 0.09 mg/cm^2 and ~200 mA/cm^2 at 0.8V with 0.36 mg/cm^2 using pure hydrogen gas and air as the reactants. Using pure hydrogen and pure oxygen gases, the 0.36 mg/cm^2 cathode was capable of achieving 1 A/cm^2 at 0.74V, which is ~30 mV less than the state-of-the-art at the time of publication [34]. Around the same time, Benitez et. al also produced PEMFC electrodes using the electrospray process; these electrodes contained 0.5 mg/cm^2 and achieved twice the power density of commercial cathodes [35][36].

Chaparro et. al further studied the electrospray process applied to PEMFC's and discovered that electrospray generates a dendritic morphology in fuel cell electrodes which increases the porosity of the catalyst layer in comparison to other deposition processes. Furthermore, Chaparro et. al demonstrated that electrosprayed catalyst layers have larger electrochemical active areas compared to other processes, at least until 30% Nafion content is reached. With a Pt loading of 0.17 mg/cm^2, the cathode was capable of achieving 25 mA/cm^2 at 0.9V using H_2/O_2 and 1 A/cm^2 at ~0.55V [37].

Chaparro et al. released another work in 2009 which investigated the optimization of catalyst load and ionomer content. They found the optimum catalyst load of 0.17 mg/cm^2 from their study to be similar to other works; however, the Nafion content in their study was found to be optimized at ~15% [38], which is far less than the 30%-40% expected from conventional wisdom of fuel cell electrode manufacturing.

Martin et al. released a study in 2010 which displayed the results of electrodes manufactured with catalyst loadings as low as 0.10 to 0.0125 mg/cm^2. In their study, they investigated the effect of Nafion content on the performance of the fuel cell with varying Pt loading, and they found that while the optimum Nafion content varied by the Pt loading, the general range was between 30% and 40%. Furthermore, Martin et al. also demonstrated that the extremely low Pt-loading of 0.0125 mg/cm^2 provided extremely low performance [39]. Martin et al. also investigated the platinum utilization of cathodes prepared by electrospraying, showing that the electrospray process is capable of achieving the same low Pt loading and Cathodic specific power as sputtering, which was a state-of-the-art Pt loading process at the time of publication [40]. An additional work by Martin et al. in 2013 further displayed the capabilities of the electrospray method to produce high-utilization ultra-low loading PEMFC electrodes [41], but, based on the metrics put forth by the US Department of Energy, the MEA's manufactured by Martin et al. display lower performance than Baturina and Wnek's in terms of current and power density. A work by Martinez-Vazquez released in 2015 investigated the "scale-up" capabilities of ultra-low Pt loading electrosprayed electrodes, which produced a 25 cm^2 electrode with performance similar to Baturina and Wnek's electrode(s) but with only 0.02 mg/cm^2. [42]

Chapter 2: Experimental Section

2.0 Experimental

Electrodes were fabricated using a lab-scale electrospray system. The system uses a Computer Numerically Controlled (CNC) table to automate movement of the target during electrospray. The use of the CNC table allows steady movement of the target and assists in producing a uniform catalyst layer on the GDL. This approach is suitable for larger electrode fabrication though longer spray times are required for large area cell fabrication.

The catalyst ink used for electrospraying of electrodes was optimized for the aforementioned electrospraying system. As discussed in Section 1.2.5.5, several parameters affect the electrospray process and conductivity of the liquid being electrosprayed is a key component. Since equipment to determine conductivity of the catalyst ink was not on-hand, a 2k factorial experiment was carried out to determine which combination of the ink components was most suitable for consistent electrospraying process.

Additionally, in an effort to validate the performance of the electrodes fabricated with the aforementioned electrospray system and also improve the performance of MEAs using the same electrodes, another 2k factorial experiment was performed on the effect of the hot pressing parameters to determine effect of pressure, time, and temperature on the performance of MEAs.

2.1 Materials for electrodes and MEAs fabrication:

Platinum on carbon black (20 wt% Pt/C, Alfa Aesar), Nafion solution (20wt%, DuPont D2021), isopropyl alcohol (Macron 3032), deionized water (Synergy UV-R Water Purification System), membrane used in this study (Nafion 212, DuPont), and gas diffusion layer (carbon paper, Sigracet).

2.2 Fabrication of electrodes and MEAs

Electrodes were fabricated via the electrospray method discussed in Section 1.2.5.4; however, some optimization of the liquid (i.e., catalyst ink) composition which was electrosprayed had to be conducted since equipment was not readily available to determine its conductivity. Enhancements to the MEA fabrication process of hot pressing were also studied to determine if an optimum combination of pressure, time, and temperature at hot pressing could be achieved for a specific MEA operating condition.

2.2.1 Optimization of Catalyst Ink and Electrode Fabrication through Electrospraying Process

As mentioned previously, electrical conductivity of a liquid used in electrospray (or named ink in this work) has an ample effect on the behavior of the spray as well as morphology of the final sprayed layer. However, effectively generating three-phase boundary within electrode with proper combination of catalyst dispersed electron-conductive carbon and accurate amount of ionomer for transporting the counter ion, and at the same time adjusting the sufficient electrical conductivity for electrospraying for a

uniform thin layer makes the task more multifaceted. Additionally, direct conductivity measurement of the ink for electrospray is not ideal due to the presence of Nafion. Therefore, a 2k factorial approach was employed for preparing uniform microporous layers around 30 um thin exhibiting appropriate electrical conductivity required for electrospraying process, which is explained further in this section. The 2k factorial experiment was designed for obtaining the uniform film within the limitation of the four ink components of Carbon, Water, Isopropyl Alcohol (IPA), and Nafion for creating the sufficient three-phase boundary for acceptable cell performence. It should be noted that catalyst such as Pt/C was not included in the optimization due to cost, and the results of the optimization were used to assist in formulating catalyst ink for electrospray. The inks used for the optimization are noted as "carbon ink" to designate them separate from "catalyst ink" which contains Pt/C. To determine the amounts of the aforementioned carbon ink components which resulted in the most uniform layer, the components were combined in varying amounts and then each combination was electrosprayed to determine the impact on the final electrosprayed coating. The combinations (called "Treatments") are provided in Table 1 on the next page. Results of the optimization are discussed in Chapter 3.

Table 1: Carbon Ink Optimization Treatments

Treatment No.	Carbon (mg)	Water (mL)	IPA (mL)	Nafion (mL)
1	225	0.9	3.75	3.75
2	275	0.9	3.75	3.75
3	225	1.1	3.75	3.75
4	275	1.1	3.75	3.75
5	225	0.9	4.25	3.75
6	275	0.9	4.25	3.75
7	225	1.1	4.25	3.75
8	275	1.1	4.25	3.75
9	225	0.9	3.75	4.25
10	275	0.9	3.75	4.25
11	225	1.1	3.75	4.25
12	275	1.1	3.75	4.25
13	225	0.9	4.25	4.25
14	275	0.9	4.25	4.25
15	225	1.1	4.25	4.25
16	275	1.1	4.25	4.25

After optimizing the carbon ink composition for electrospray, electrode catalyst ink were prepared by dispersing 20 wt% Pt/C in isopropanol, deionized water, and Nafion. The ultimate catalyst loadings for anode and cathode were approximately 0.06 mg/cm^2 and 0.10 mg/cm^2, respectively.

2.3 Electrode Fabrication

Electrodes were fabricated similarly to [39] by electrospraying the catalyst ink through a 5 mL glass syringe (Fortuna SYR-GL5LL) feeding a Nylon tube to an 18-

gauge stainless steel needle (Sodial) with nominal dimensions of 0.57mm ID X 1.18mm OD X 1” Length. The glass syringe was powered by a syringe pump (NE-300 model, New Era). Potential difference to form the Taylor Cone necessary for electrospraying was achieved with a high voltage power supply (H101P, EMCO High Voltage Corporation) attached to the stainless steel needle. A computer-numerically controlled (CNC) machine (Shapeoko 2, Inventables) was modified to create an automated stage used to ensure uniformity of catalyst layers.

The catalyst ink was electrosprayed at a positive voltage of 9.2 kV, needle to stage height of 3.5 cm, and flowrate of 0.2 uL/min. Time of electrospray deposition varied between 30 minutes and 1 hour to achieve loadings of 0.06 mg/cm^2 and 0.10 mg/cm^2, respectively, on 5 cm^2 anode and cathodes. These catalyst loadings were chosen to approach the US Department of Energy's Technical Targets for Polymer Electrolyte Membrane Fuel Cell Components for 2020, which is set to 0.125 mg/cm^2 total loading for both anode an cathode.

2.4 MEA Preparation and Optimization of Lamination Process

MEAs were hot pressed in a hydraulic press (Carver 3925) with varying levels of the three critical parameters: 1) Pressure, 2) Temperature, and 3) Time. Review of literature related to electrosprayed electrodes and hot-pressed MEAs revealed different values of these three parameters applied by different works - with MEAs using non-electrosprayed electrodes varying further. Table 2 below shows examples of the values for pressure, time, and temperature applied by other works as well as values applied to

airbrushed electrodes [14]. Electrodes fabricated via electrospray are expected to have higher porosity than those prepared by other means [43] allowing for better transport of reactants and product from/to reaction sites, resulting in higher performance [44][45]. Values for the hot-pressing parameters 2k factorial experiment were selected by comparing pressures, times, and temperatures from the works listed in Table 2 to determine the lowest and highest values. The highest pressure applied (8 MPa) was selected to stay within the upper limit of the hydraulic press gauge, though the value is relatively similar to those used by the other studies so it will approximate a similar reesult. The lowest temperature applied (110°C) was selected to understand the impact of pressing temperature below the `commonly applied temperature of ~120°C. The pressure, time, and temperature applied to specific MEAs from the experiment are listed in Table 3.

Table 2: ***Comparison of hot pressing pressures, times and temperatures***

Study	Electrode Fabrication	GDL Type	Electrode Area (cm^2)	Pressure (MPa)	Time (sec)	Temperature (°C)
S. Martin et al. 2010 [28]	Electrospray	Carbon Paper	5	10	120	120
S. Martin et al. 2010 [29]	Electrospray	Carbon Paper	5	5	120	120
Chaparro et al. 2005 [33]	Electrospray	Carbon Cloth	29.2	18.8	180	120
Tang et al. 2007 [46]	Screen Printing	Carbon Paper	25	10	90	125
Bose et al. [14]	Airbrushed	Carbon Paper	5	2.67	390	150

Table 3: **Pressure, time, and temperatures applied to each MEA**

MEA #	Pressure (MPa)	Time (seconds)	Temperature (°C)
MEA2K1	2.67	90	110
MEA2K2	8	90	110
MEA2K3	2.67	390	110
MEA2K4	8	390	110
MEA2K5	2.67	90	150
MEA2K6	8	90	150
MEA2K7	2.67	390	150
MEA2K8	8	390	150

2.5 MEA Testing and Characterization

MEAs were tested to characterize the electrodes via MEA performance, and also to validate the electrode fabrication system. Furthermore, since the electrode catalyst loadings were chosen to approach the US Department of Energy's 2020 target of 0.125 mg/cm^2 (total loading for both electrodes), MEA testing also provided information on performance of the MEAs/electrodes relative to the target.

2.5.1 Polarization Curve and Losses

Polarization losses or polarization overpotential are irreversible losses in cell potential [47] (voltage) relative to the theoretical potential, which a fuel cell incurs at specific stages of operation. The polarization curve - or i-V curve - summarizes the performance of a cell by showing the voltage output of a cell at a certain current output normalized by electrode surface area. The three main types of losses are: 1) activation polarization, 2) ohmic polarization, and 3) mass transport polarization [48].

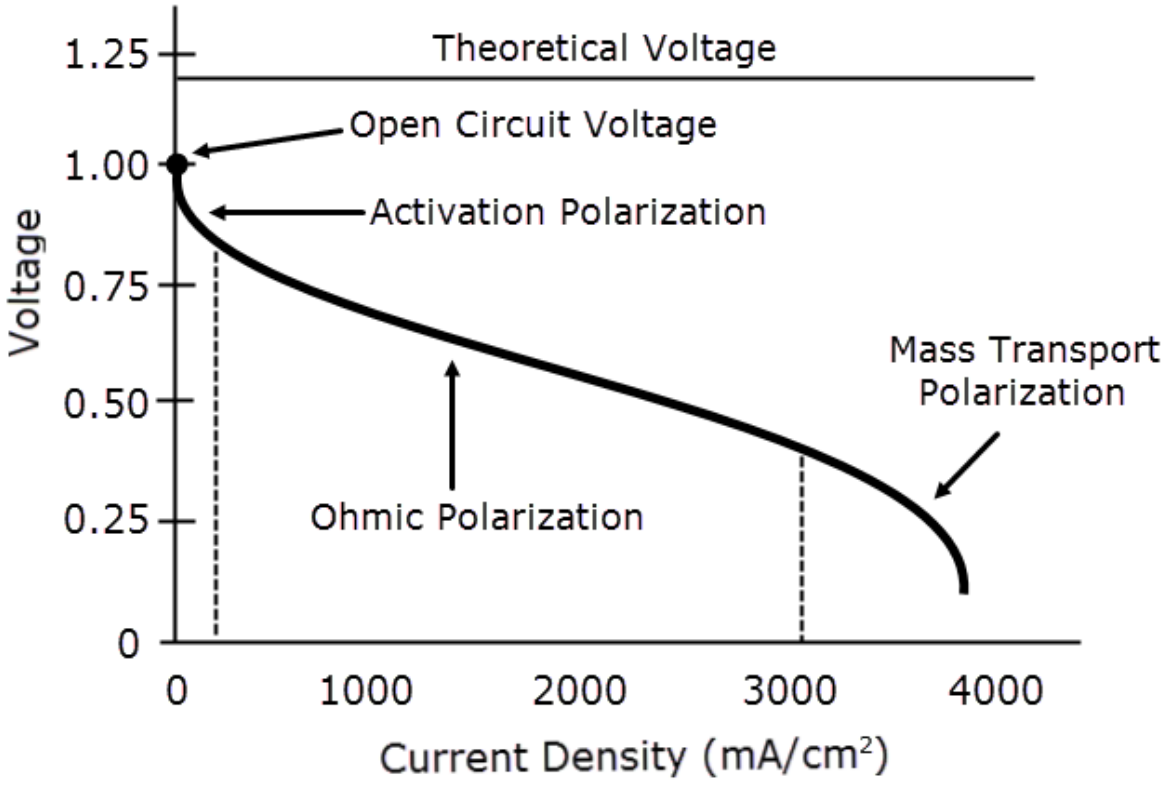

Figure 9: ***Example polarization curve with polarization regions indicated***

The cell voltage can be represented by the reversible voltage minus the three types of losses mentioned above:

$$V_{cell} = E_{theor} - \eta_{act} - \eta_{ohm} - \eta_{conc}$$

Where,

V_{cell} = Cell voltage

E_{theor} = Reversible Voltage

η_{act} = activation losses

η_{ohm} = ohmic losses

η_{conc} = concentration (or "mass transport") losses

Activation losses occur and dominate in the low current density region (up to ~150 mA/cm^2) and are the voltage lost to overcome the activation barrier. For a PEMFC, the anodic reaction kinetics are typically neglected since the losses for the hydrogen reaction are insignificant in comparison with the oxygen reaction on cathodic side of the fuel cell. Kinetic performance can be increased by: 1) increasing reactant concentration, 2) decreasing activation barrier, 3) increasing temperature, and 4) increasing reaction sites [48].

As current density increases and a fuel cell's operation exits the low current density region, ohmic losses begin to take effect. Ohmic losses are due to the resistance in charge transport of the electrons and protons through the fuel cell's MEA

and other components. This loss is termed "ohmic" loss because it obeys Ohm's law [49].

As much higher currents are elicited from the fuel cell, mass transport losses begin to take effect. Mass transport losses in the electrodes relate to both the supply of reactants to and removal of products from the fuel cell reaction sites. These losses are due to a combination of reactants being consumed faster than can be supplied from the bulk media and products not exiting the reaction sites quickly, further preventing reactants from reaching reaction sites.

MEA testing was evaluated via a fuel cell test station (850e, Scribner Associates). Polarization curves were obtained using Ultra High Purity Hydrogen and Oxygen gases fed to the anode and cathode, respectively, at flow rates of 0.2L/min for both. Performance testing was performed at operating temperatures of 60°C and 80°C. Testing was performed with two combination of RH for the feed gases: 1) 50% RH on the anode and 25% RH on the cathode (which is denoted as "50%-25% RH"), and 2) 100% RH on both the anode and cathode (which is denoted as "100% RH"). Polarization data was obtained by performing a current scan starting from Open Circuit Voltage (OCV) to 0.4V at steps of 0.2A held for 2 minutes at each point.

Table 4: Operating temperatures and relative humidity conditions for MEA testing

Operating Temperature	Anode Relative Humidity	Cathode Relative Humidity
60°C	50%	25%
	100%	100%
80°C	50%	25%

	100%	100%

Humidification of the reactant gases was calculated automatically through the Scribner 850e, which calculates percent humidification with the following equations:

$$\%\ RH = \frac{Anode\ or\ Cathode\ Humidifier\ Water\ Vapor\ Pressure}{Cell\ Water\ Vapor\ Pressure} * 100$$

$$Water\ Vapor\ Pressure = (1.2282 * 10^{-8})T^4 - (9.3703 * 10^{-7})T^3 + (7.7644 * 10^{-5})T^2 - (7.9482 * 10^{-4}) + (1.0290 * 10^{-2})$$

Where T = temperature (in °C) of the anode, cathode, or cell

2.5.1 Cyclic Voltammetry

Cyclic voltammetry was performed to determine the electrochemical surface area (ECSA) of the electrode. This technique is performed by sweeping an MEA between two voltages and simultaneously recording the current [49]. The resulting plot of voltage versus current contains various peaks which indicate electrochemical reactions occurring at certain voltages. The peaks of interest for ECSA in this instance, are those related to hydrogen desorption, and the area beneath these peaks can be calculated and converted to ECSA if the time is known [50].

$$ECSA = \frac{q}{\Gamma * L}$$

Where

q = charge density in C/cm^2

Γ = charge to reduce monolayer of protons on Pt (210 uC/cm^2)

L = Pt content of the electrode in g Pt/cm^2)

Cyclic Voltammetry was performed using a frequency response analyzer (Solartron 1260) with an electrochemical potentiostat/galvanostat (Solartron SI 1287). Voltage sweeps were performed from 0 V to 0.8 V at a rate of 40 mV/s. Feed gases were Ultra High Purity Hydrogen and Nitrogen fed to the anode and cathode, respectively, at flow rates of 0.2L/min and 100% RH for both.

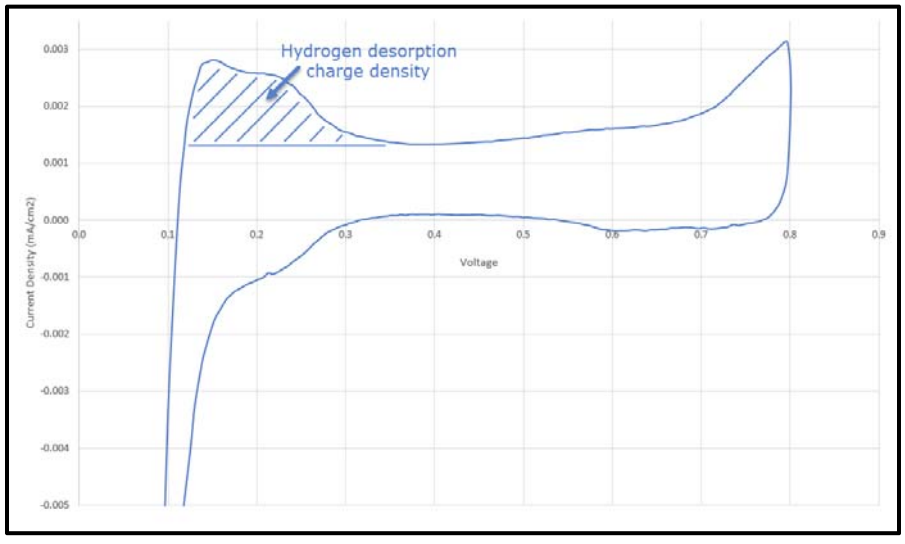

Figure 10: Experimentally collected CV curve illustrating hydrogen desorption charge density for ECSA calculation

3.0 Results and Discussion

A number of MEAs with similarly identical catalyst and ionomer compositions as specified as catalyst ink were prepared under different hot pressing conditions and their performances were evaluated. Both the catalyst ink and hot pressing parameters are explained in sections 2.2.1 and 2.4, respectively. A total of eight MEAs were prepared with same ink composition but varying hot pressing parameters. This section explains the factors to achieving uniform thin electrode layer, and effect of hot pressing parameters on MEA fabrication and cell performance.

3.1 Carbon Ink Optimization

Carbon ink composition was optimized for consistent cone-jet mode spraying at a specific needle-to-target height of 3.5 cm, voltage of 9.2 kV, and flow rate of 2.0 uL/min. Although the final fuel cell electrode ink uses platinum-on-carbon (Pt/C) catalyst in place of plain carbon, the initial optimization was carried out with plain carbon to reduce waste of valuable Pt/C. Each treatment of the 2k factorial experiment is shown in Table 5 below. Each treatment was electrosprayed for at least 20 minutes onto a stage, and the stage was translated every 2 minutes to capture any changes in the number of jets emitting ink from the needle. The number of jets was easily determined by counting the distinct regions visible in each 2-minute long spray. See Figure 11 on the next page for examples of the sprayed regions produced by cone-jet mode and others. The spray results from each treatment were evaluated by averaging the number of jets per

sprayed cluster over the total number of clusters sprayed - values were captured as "Jet Average Over Time".

Table 5: Treatment numbers and corresponding component amounts plus jet average over time

Treatment No.	Carbon (mg)	Water (mL)	IPA (mL)	Nafion Solution (mL)	Jet Average Over Time
1	225	0.9	3.75	3.75	5
2	275	0.9	3.75	3.75	2.93
3	225	1.1	3.75	3.75	2
4	275	1.1	3.75	3.75	2.8
5	225	0.9	4.25	3.75	3.2
6	275	0.9	4.25	3.75	4.36
7	225	1.1	4.25	3.75	1.33
8	275	1.1	4.25	3.75	4.71
9	225	0.9	3.75	4.25	2.86
10	275	0.9	3.75	4.25	2.69
11	225	1.1	3.75	4.25	3
12	275	1.1	3.75	4.25	2.25
13	225	0.9	4.25	4.25	1
14	275	0.9	4.25	4.25	4.36
15	225	1.1	4.25	4.25	4.22
16	275	1.1	4.25	4.25	4.11

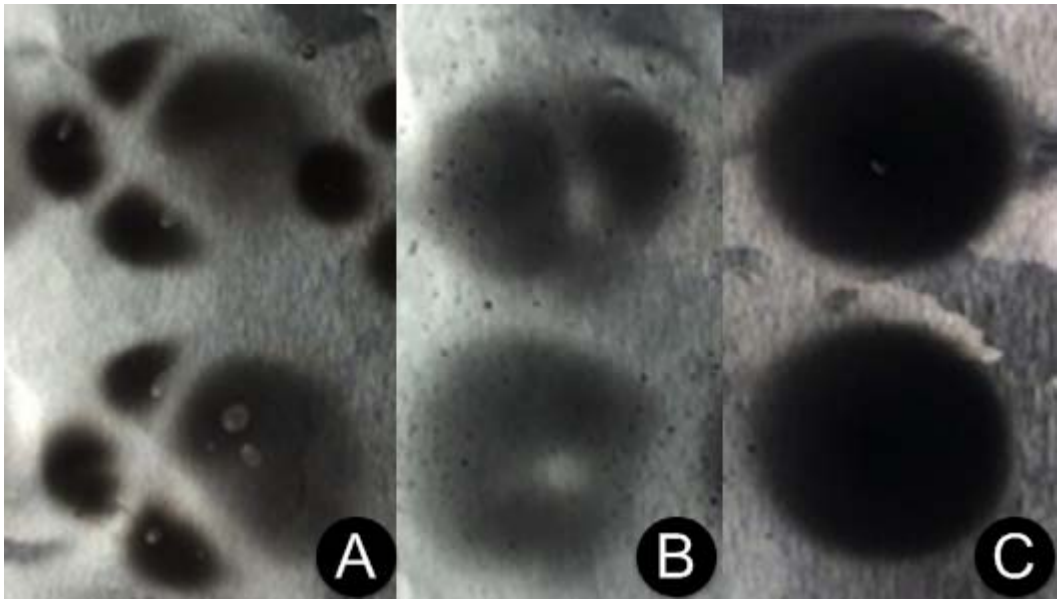

Figure 11: ***Spray results showing multi-jet and cone-jet sprayed regions - each cluster electrosprayed for 2 minutes. A) Sample of multi-jet result from Treatment 16, B) Sample of multi-jet result from Treatment***

Although the number of jets could vary over time due to variations in output voltage from the high voltage power supply, the variation was not overly significant for any of the treatments. By optimizing the ink composition to determine which could be electrosprayed the most stably, the resulting ink conductivity is such that the cone-jet mode can persist for a larger range within the power supply's voltage variations.

The main effects plot from the 2k factorial experiment shown in Figure 12 demonstrates that increases in carbon amount from 225 mg to 275 mg and IPA amount from 3.75 mL to 4.25 mL increases the number of jets generated by the electrospray. Meanwhile, increases in the amount of water from 0.9 mL to 1.1 mL and Nafion solution from 3.75 mL to 4.25 mL results in decreasing the number of jets.

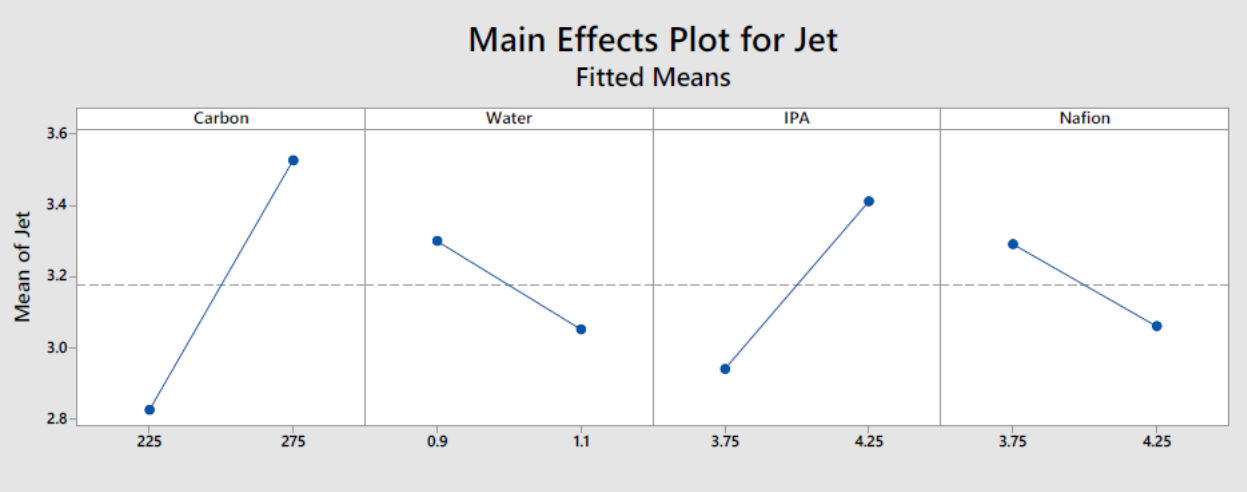

Figure 12: ***Main effects plot from ink optimization 2k factorial experiment.***

The final catalyst ink used to electrospray electrodes followed closely to the treatments with the lowest jet averages over time; though some slight variations were made to the amounts of Nafion solution and IPA since Pt/C was used instead of plain carbon.

3.2 Effect of hot pressing parameters on performance of electrosprayed electrodes

Effect of hot pressing parameters (time, temperature, and pressure) on electrosprayed electrode performance was studied via 2k factorial experiment to determine an optimum combination of the three parameters. Eight MEAs were produced, each at varying combinations of time, temperature, and pressure, and each MEA was tested at 60°C and 80°C with two conditions of relative humidity: 1) 100% RH for both the anode and cathode, and 2) 50% RH for the anode and 25% RH for the

cathode. Voltage achieved at 1 A/cm^2 current density was the benchmark of performance to which all of the tested MEA's were compared.

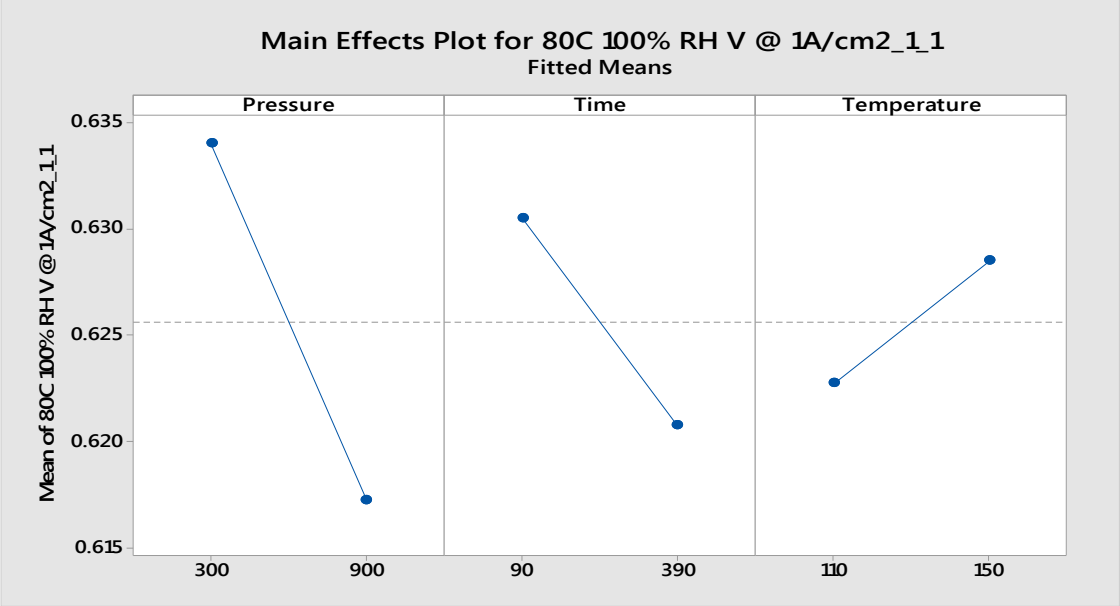

Figure 13: Main effects plot from hot pressing 2k factorial and effect on V @ 1A/cm^2 for 80°C 100% RH operating condition.

Comparison of the main effects plots for the hot pressing 2k factorial experiment at the 60°C 100% RH and 80°C 100% RH conditions (Figures 13 and 14), shows similar effects on the voltage achieved at current density of 1A/cm^2. In summary, increases in the applied pressure during hot pressing and amount of time for hot pressing results in reduction of the voltage, while increase in the hot pressing temperature results in an increase in voltage. The effect of increased pressure applied during hot pressing can likely be attributed to compression of the electrode porosity and was previously considered in [9], and the effect of temperature applied during hot pressing can be attributed to improved contact of the membrane with the electrodes [52].

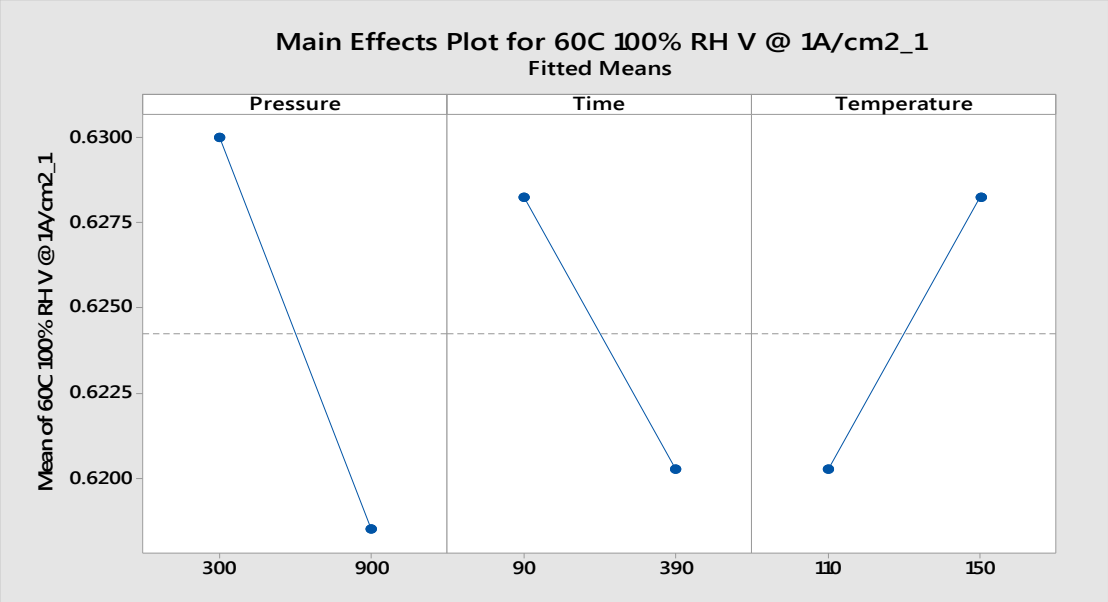

Figure 14: Main effects plot from hot pressing 2k factorial and effect on V @ 1A/cm^2 for 60°C 100% RH operating condition.

Table 6 in combination with Table 7 list the hot pressing parameters used to fabricate each MEA and also provide information garnered from testing and characterization such as current densities and power densities achieved at 0.7V and 0.6V, ECSA, etc. The calculated ECSA values correspond with the values reported in [33], which suggests that the fabricated electrode is at least up to par with previous works in the respect of platinum utilization. And though MEA2K4 is shown to have the highest ECSA value, its performance was mediocre relative to the rest of the MEA's. MEA2K4 also had the highest Tafel slope which suggests that the higher ECSA was not completely taken advantage of due to the higher activation loss. The poor performance is also attributed to the higher pressure which was applied during hot pressing, which likely compressed the pore structure within as compared to those hot-pressed at lower

pressure. It should be noted that at least some component of the ECSA variations is also due to slight variations in ink composition between MEA's.

Table 6: Summary of hot pressing parameters compared with ECSA, Tafel slope, and Open Circuit Voltages (OCV)

MEA No.	Hot Pressing Pressure	Hot Pressing Time	Hot Pressing Temp	Est. Total MEA Loading (mg/cm^2)	ECSA (m^2/g Pt)	Tafel Slope, b (mV/dec)	OCV 80°C 100% RH	OCV 60°C 100% RH	OCV 80°C 50%-25% RH	OCV 60°C 50%-25% RH
MEA2K1	2.67 MPa	90 sec	110°C	0.152	22.23	91.44	0.979	0.999	0.998	1.004
MEA2K2	8 MPa	90 sec	110°C	0.154	28.23	92.37	0.971	0.974	0.958	0.966
MEA2K3	2.67 MPa	390 sec	110°C	0.154	25.49	91.14	0.985	1.009	1.018	1.022
MEA2K4	8 MPa lbf	390 sec	110°C	0.166	30.29	99.76	0.959	0.963	0.957	0.954
MEA2K5	2.67 MPa	90 sec	150°C	0.154	27.95	92.49	0.971	0.986	0.989	0.998
MEA2K6	8 MPa lbf	90 sec	150°C	0.154	19.97	93.71	0.922	0.936	0.901	0.913
MEA2K7	2.67 MPa	390 sec	150°C	0.163	19.18	90.07	0.911	1.001	1.001	1.004
MEA2K8	8 MPa lbf	390 sec	150°C	0.160	23.96	95.64	0.925	0.944	0.913	0.929

**Anode and cathode catalyst loadings ranged from 5.1 to 6.3 and 9.7 to 10.9 mg/cm^2, respectively.*

Based on the obtained values in Table 7, it suggests that the combination of low pressure (2.67 MPa), long pressing time (390 sec), and high temperature (150°C) used to fabricate MEA2K7 produces higher (if not the highest) voltage at 1 A/cm^2 and, subsequently, the highest overall performance. This is also apparent across the four operating conditions shown in Table 7. In comparison, MEA2K8, which was hot-pressed for the same length of time at the same temperature but at a lower pressure, performed the least favorably in three of the four operating conditions.

Overall, the variation of the activation losses between the MEA's which are shown in Figures 15 through 19 seems to be minimal as evidenced by the similar transitions from the curved activation overpotential region to the linear ohmic overpotential region of each curve. This is also evidenced by the similar Tafel slopes shown in Table 6 on the previous page. The distinct differences in performance in the polarization curves are then attributed to the ohmic overpotential which is significantly affected by mass transport. While electrosprayed electrodes have been shown to have favorable mass transport morphology in general [52], the effect of hot pressing at varying conditions suggests the benefits of the electrosprayed method could be impacted by hot pressing - namely the pressure applied in the process.

Additionally, the porosity that benefits the mass transport within electrosprayed electrodes are also shown to have at least some benefit when operating in reduced relative humidity conditions. This is evidenced in Figure 19 where the 80°C 100% RH conditions for both MEA2K5 and MEA2K7 (shown in darker colors) have the best performance as expected, though, both MEA's operated at 60°C and 50%-25% RH on the anode and cathode, respectively, had only ~0.1V drop in voltage at 1A/cm^2 in

comparison. The relatively slight decrease in performance at 60°C but with much lower humidification is significant since reduction in equipment for humidification of fuel cells could contribute to reduced overall cost with similar performance.

Ultimately, it can be seen that MEA's using electrosprayed electrodes perform better at lower hot pressing pressure, and this result was corroborated by [53] for Direct Methanol Fuel Cell (DMFC) electrodes prepared via doctor blading.

Table 7: Results of hot pressing parameters compared with voltages achieved at 1A/cm²

	80C 100% RH					80C 50%-25% RH					60C 100% RH					60C 50%-25% RH				
MEA No.	**OCV**	**Current Density (mA/cm2) [Power Density] (mW/cm2) @0.7V**	**Current Density (mA/cm2) [Power Density] (mW/cm2) @0.6V**	**Peak Power Density (mW/cm2)**	**V @ 1A/cm2**	**OCV**	**Current Density (mA/cm2) [Power Density] (mW/cm2) @0.7V**	**Current Density (mA/cm2) [Power Density] (mW/cm2) @0.6V**	**Peak Power Density**	**V @ 1A/cm2**	**OCV**	**Current Density (mA/cm2) [Power Density] (mW/cm2) @0.7V**	**Current Density (mA/cm2) [Power Density] (mW/cm2) @0.6V**	**Peak Power Density**	**V @ 1A/cm2**	**OCV**	**Current Density (mA/cm2) [Power Density] (mW/cm2) @0.7V**	**Current Density (mA/cm2) [Power Density] (mW/cm2) @0.6V**	**Peak Power Density**	**V @ 1A/cm2**
MEA2K1	0.979	520 [365]	1200 [365]	954	0.628	0.999	160 [113]	360 [216]	453	0.425	0.999	560 [393]	1160 [697]	953	0.627	1.004	240 [169]	680 [407]	825	0.564
MEA2K2	0.971	520 [366]	1200 [366]	990	0.629	0.958	160 [113]	360 [218]	440	0.421	0.974	560 [392]	1120 [672]	933	0.620	0.966	240 [168]	600 [359]	766	0.538
MEA2K3	0.985	520 [365]	1200 [722]	965	0.629	0.901	200 [139]	440 [261]	520	0.458	0.936	560 [391]	1120 [674]	933	0.621	1.022	240 [168]	640 [383]	800	0.553
MEA2K4	0.894	560 [392]	1240 [747]	1046	0.636	0.957	160 [112]	440 [262]	424	0.413	0.963	560 [393]	1160 [697]	980	0.626	0.954	280 [195]	680 [410]	865	0.562
MEA2K5	0.971	520 [365]	1320 [794]	1160	0.638	0.989	160 [113]	440 [262]	572	0.463	0.986	560 [393]	1280 [766]	1112	0.636	0.998	240 [170]	760 [456]	932	0.573
MEA2K6	0.922	480 [337]	1200 [722]	1070	0.627	0.901	200 [139]	440 [262]	520	0.458	0.936	560 [391]	1200 [720]	1062	0.628	0.913	240 [169]	640 [385]	905	0.557
MEA2K7	0.911	560 [391]	1320 [794]	1130	0.641	1.001	200 [138]	440 [262]	571	0.469	1.002	600 [418]	1280 [765]	1097	0.636	1.004	280 [195]	800 [477]	935	0.575
MEA2K8	0.925	440 [308]	1040 [626]	903	0.608	0.913	160 [113]	440 [262]	459	0.433	0.944	520 [363]	1080 [648]	954	0.613	0.929	240 [168]	600 [359]	766	0.535

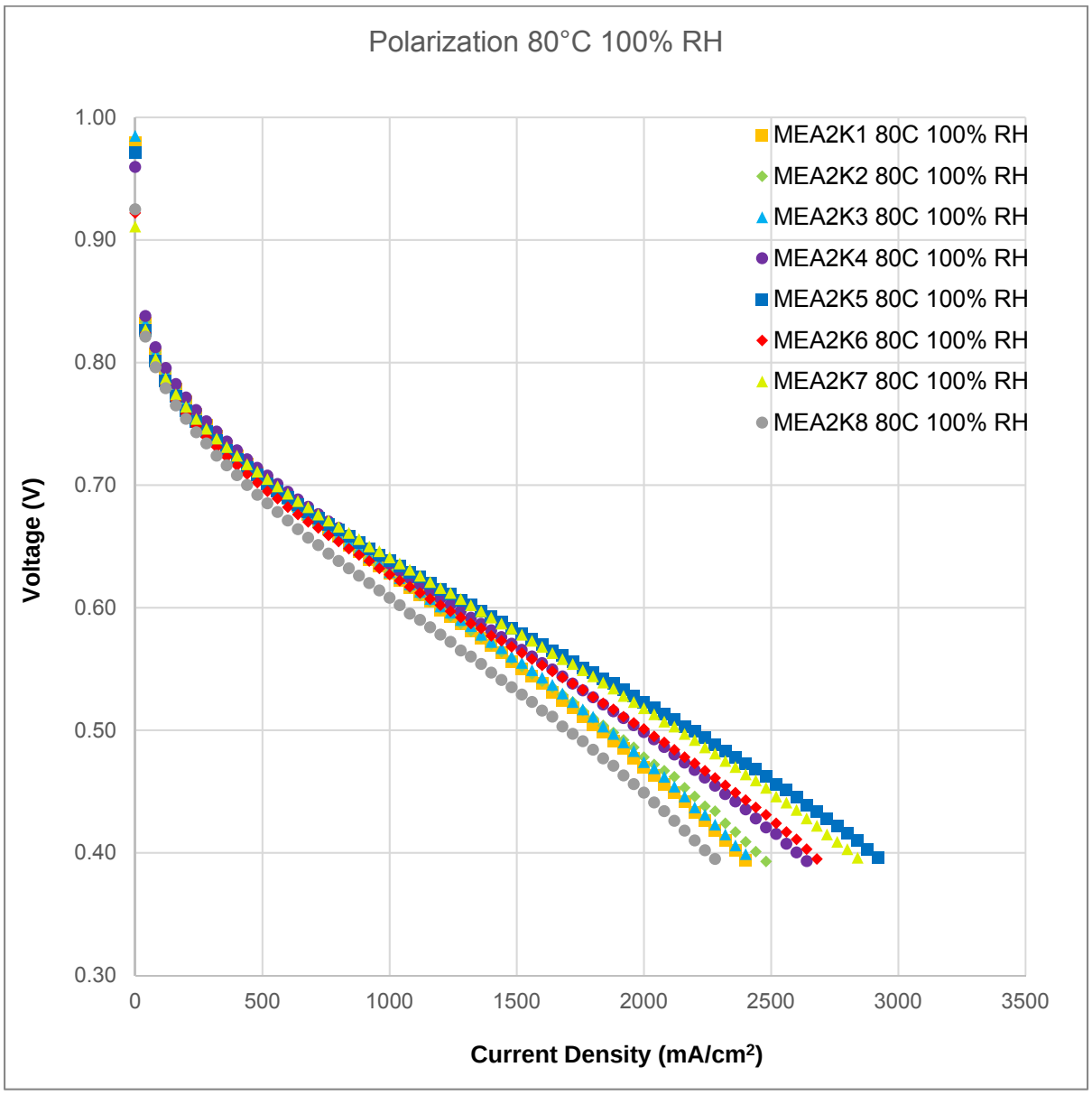

Figure 15: Polarization curves at 80°C and 100% RH on both anode and cathode.

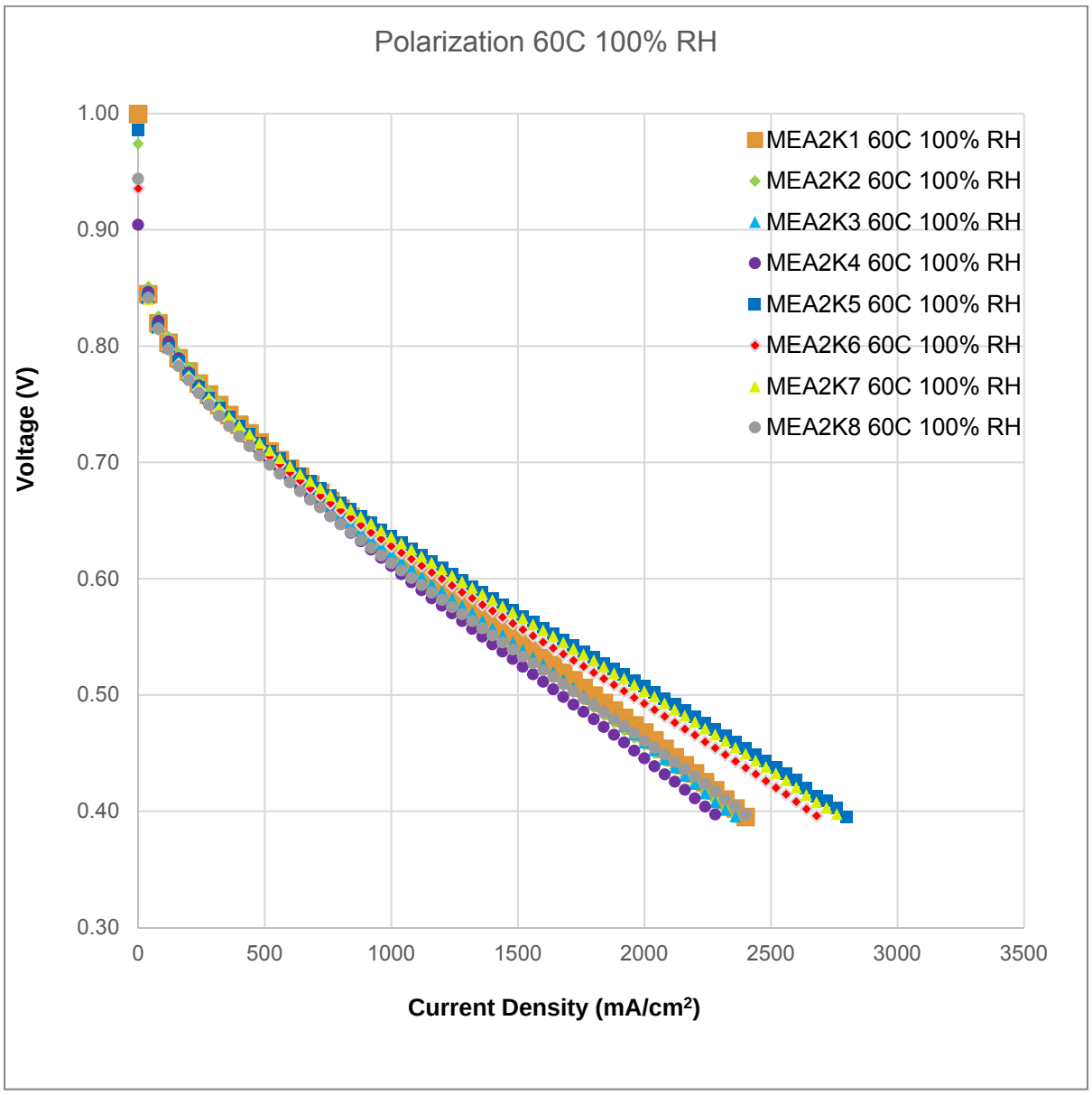

Figure 16: Polarization curves at 60°C and 100% RH on both anode and cathode.

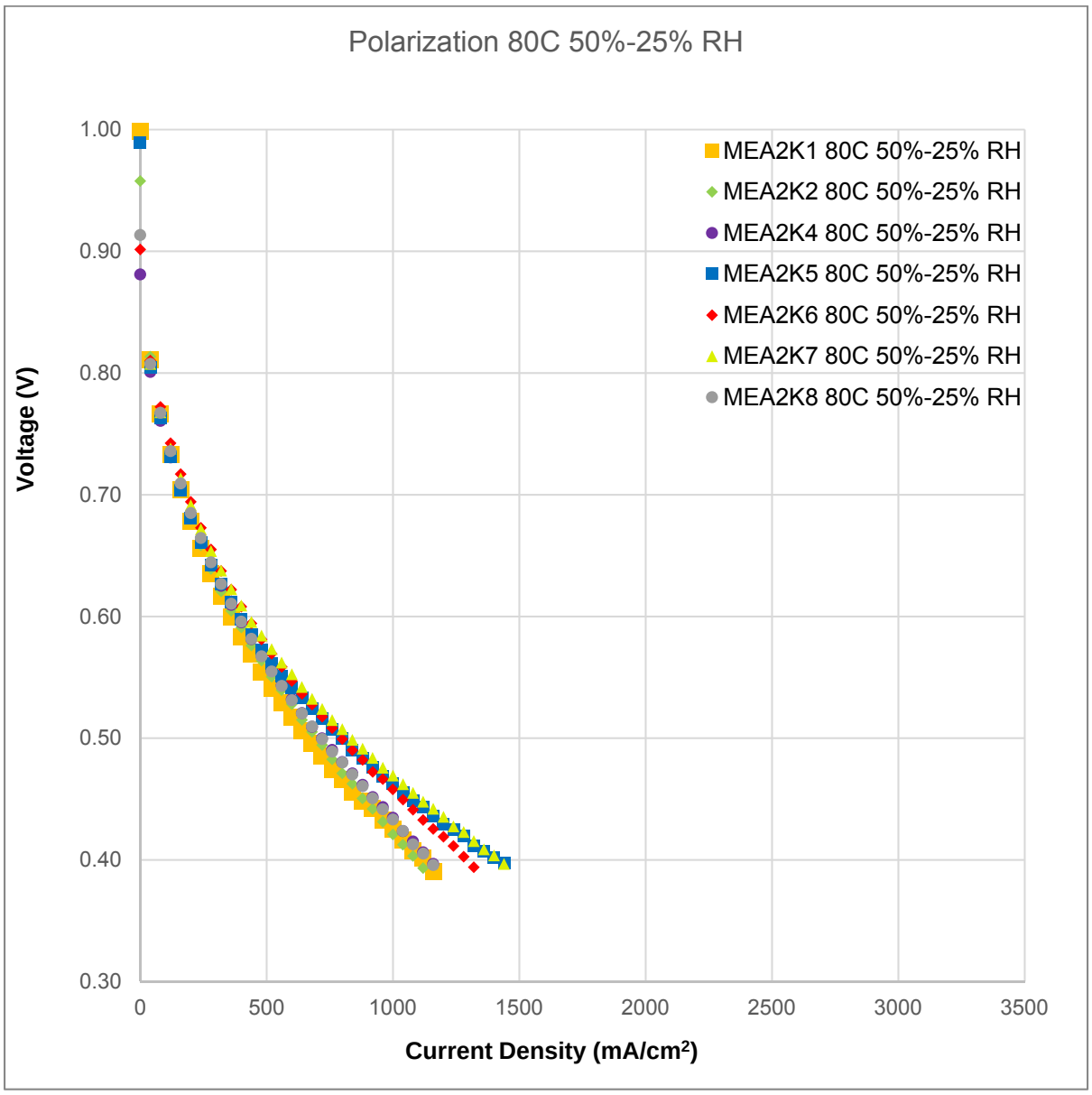

Figure 17: Polarization curves at 80°C and 50% RH on the anode and 25% RH on anode

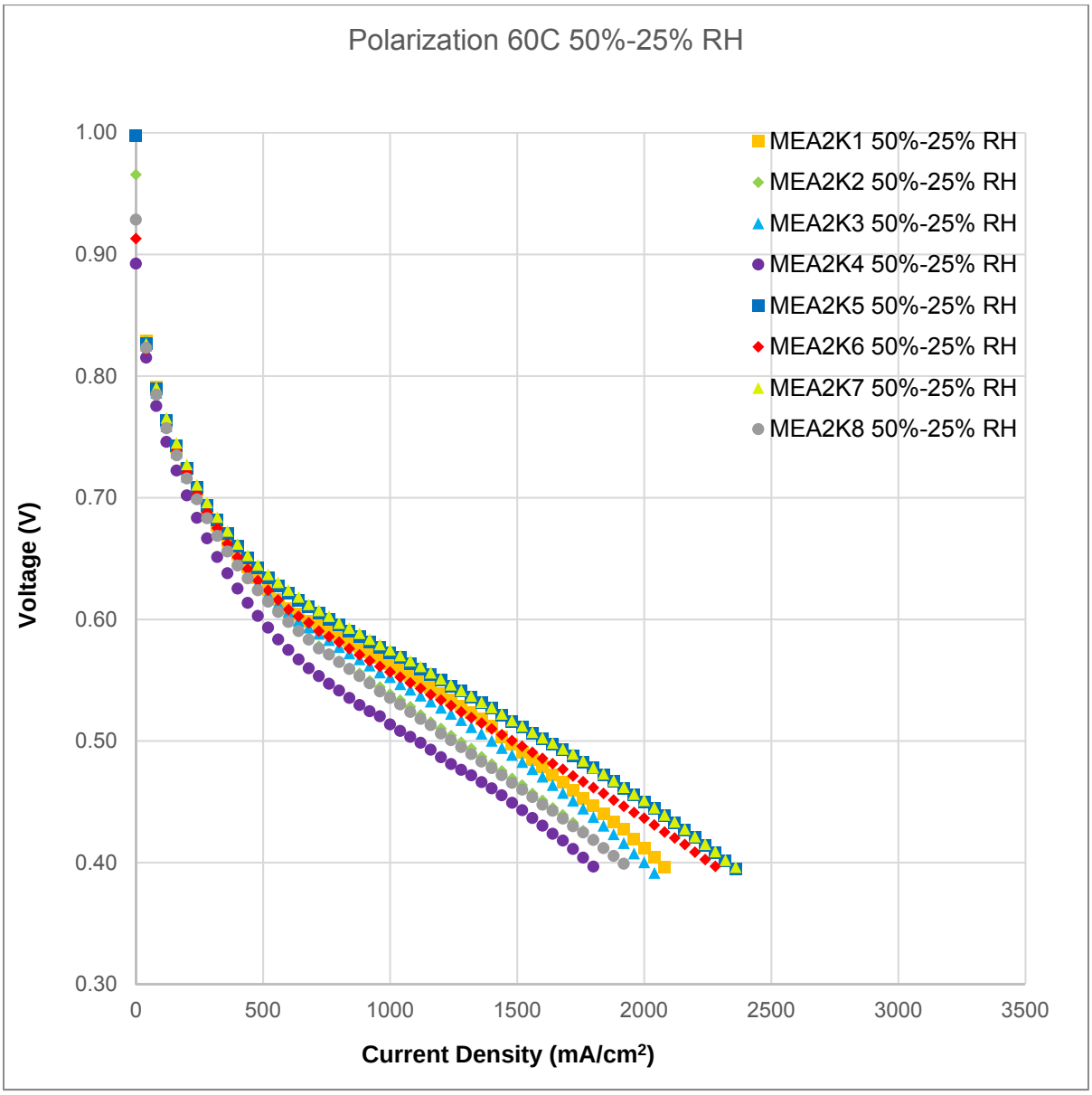

Figure 18: Polarization curves at 60°C and 50% RH on the anode and 25% RH on anode

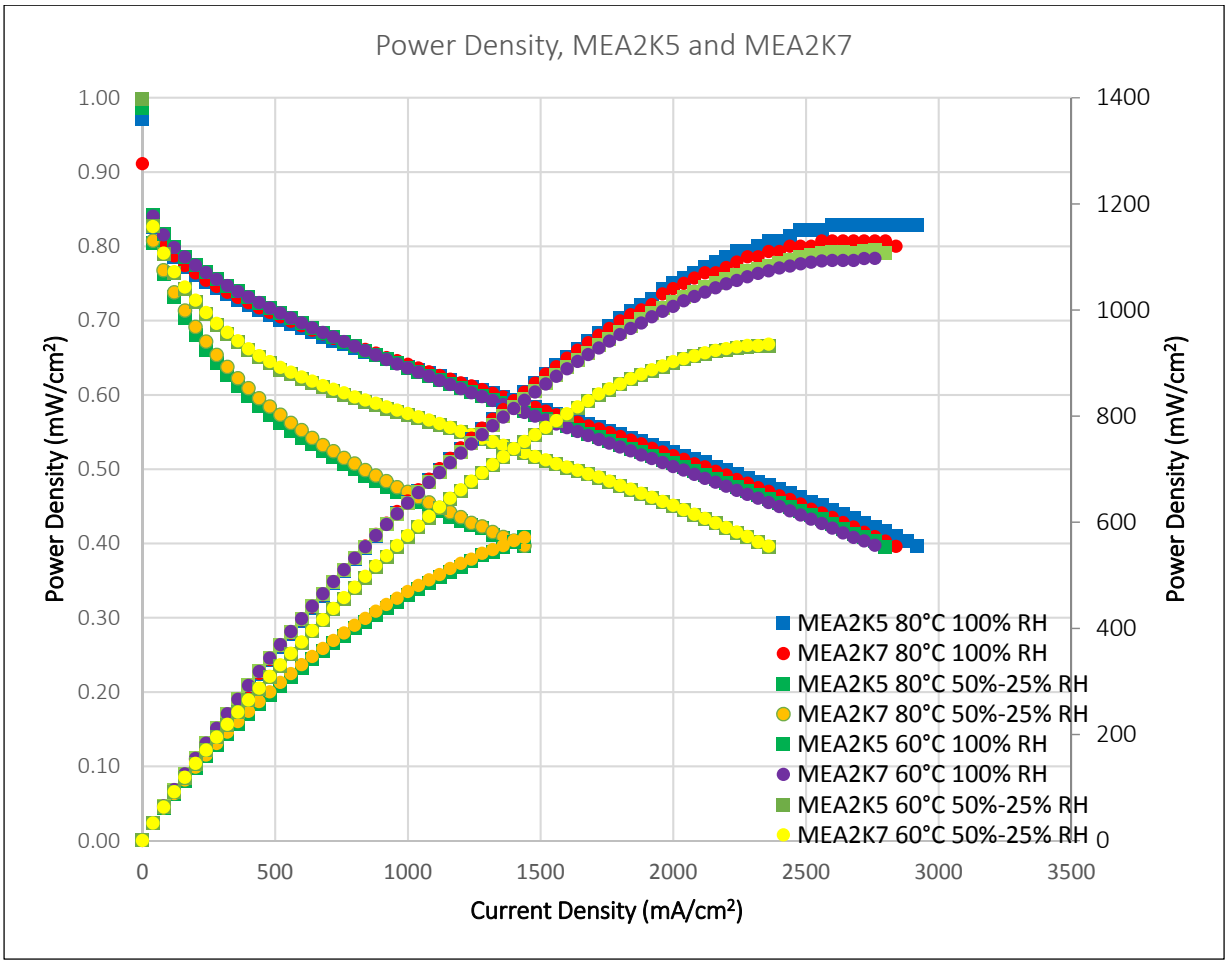

Figure 19: Comparison of MEA2K5 and MEA2K7 polarization and power density curves at all operating conditions

4.0 Conclusion

Fuel cell electrodes fabricated via electrospray exhibit several favorable characteristics such as high catalyst utilization and high porosity which could contribute to achieving the US Department of Energy's 2020 target of reducing PEFMC catalyst loadings to 0.125 mg/cm^2. An electrospray system was built to fabricate fuel cell electrodes and study improvements related to these electrodes, such as the effect of hot pressing on the performance of the electrodes as part of membrane electrode assemblies. A 2k factorial experiment was conducted to assist in determining an optimum combination of pressure, time, and temperature for hot-pressing of MEA's, and said MEA's were characterized by polarization at 60°C and 80°C with relative humidity of either 50% on the anode and 25% on the cathode or 100% for both. Cyclic voltammetry was also performed to determine electrochemical surface area for each electrode.

Results of performance testing of MEAs from this study showed that the electrodes fabricated by the aforementioned electrospray system perform better when pressed at a low pressure. This is readily seen when comparing MEA2K4, which had the highest ECSA and would be expected to have the highest performance but pressed at a high pressure, with MEA2K7, which had a lower ECSA but pressed at a lower pressure. The result is even more stark when comparing MEA2K7 and MEA2K8, both essentially pressed the same except for the different pressures, and yet MEA2K8 actually performed the least favorably for the majority of operating conditions

The best combination of hot-pressing parameters found in this study is: 2.67 MPa pressure, 90 sec pressing time, and 150°C pressing temperature. Additionally, the

electrosprayed electrodes fabricated in this study showed promising results regarding reduced humidification operating conditions with only a slight reduction in performance relative to 100% relative humidity operating conditions. This result is especially significant for further reducing the cost of a fuel cell stack by reducing the humidification equipment for operation.

As a continuation of this study, another 2k factorial experiment with larger area electrodes can be tested to observe if the size of the electrode has a significant effect on an optimum hot pressing combination. The results will be useful in larger scale applications such as vehicle operation. Physical evaluation of the catalyst layer morphology should also be conducted via SEM before hot-pressing, after hot-pressing, and after the MEA has been removed from test equipment to examine micro-structure after each process.

References

1. S. Chalk, J. Miller, F. Wagner, Challenges for fuel cells in transport applications, Journal of Power Sources, 86 (2000) 40-51
2. Clement-Nyns, Kristien, Haesen, Edwin, & Driesen, Johan. (2010). The Impact of Charging Plug-In Hybrid Electric Vehicles on a Residential Distribution Grid. *IEEE Transactions on Power Systems, 25*(1), 371-380.
3. T. Yoshida, K. Kojima, Toyota Mirai Fuel Cell Vehicle and Progress Toward a Future Hydrogen Society, The Electrochemical Society Interface, (2015) 45-49.
4. J.H. Wee, Applications of proton exchange membrane fuel cell systems, Renewable and Systainable Energy Reviews, 11 (2007) 1720-1738
5. F. Barbir, T. Gomez, Efficiency and Economics of Proton Exchange Membrane (PEM) Fuel Cells, International Journal of Hydrogen Energy,
6. D. Chu, R. Jiang, K. Gardner, R. Jacobs, J. Scmidt, T. Quakenbush, J. Stephens, Polymer electrolyte membrane fuel cells for communication applications, Journal of Power Sources, 96 (2001) 174-178
7. G. Wu, K.L. More, C.M. Johnston, P. Zelenay, High-Performance Electrocatalysts for Oxygen Reduction Derived from Polyaniline, Iron, and Cobalt, Science, 332 (2011) 443-447
8. V.A. Paganin, E.A. Ticianelli, E.R. Gonzalez, Development and electrochemical studies of gas diffusion electrodes for polymer electrolyte fuel cells, Journal of Applied Electrochemistry, 26 (1996) 297-394
9. M.S. WIlson, S. Gottesfeld, Thin-film catalyst layers for polymer electrolyte fuel cell electrodes, 22 (1992) 1-7

10. C.S. Kim, Y.G. Chun, D.H. Peck, D.R. Shin, A novel process to fabricate membrane electrode assemblies for proton exchange membrane fuel cells, Int. Jour. Hyd. Energy 11 (1998) 1045-1048
11. A.M. Chaparro, R. benitez, L. Gubler, G.G. Scherer, L. Daza, Stufy of membrane electrode assemblies for PEMFC with cathodes prepared by the electrospray method.
12. S. Martin, P.L. Garcia-Ybarra, J.L. Castillo, Electrospray deposition of catalyst layers with ultra-low Pt loadings for PEM fuel cells cathodes, Journal of Power Sources, 195 (2010) 2443-2449
13. T. Wilberforce, A. Alaswad, A. Palumbo, M. Dassisti, A.G. Olabi, Advances in stationary and portable fuel cell applications, International Journal of Hydrogen Energy, 41 (2016) 16509-16522
14. A.B. Bose, R. Shaik, J. Mawdsley, Optimization of the performance of polymer electrolyte fuel cell membrane-electrode assemblies: Roles of curing parameters on the catalyst and ionomer structures and morphology, Journal of Power Sources, 182 (1) 61-65
15. C.S. Spiegal, Designing and Building Fuel Cells, first ed., 2007, McGraw-Hill
16. X. Cheng, B. Yi, M. Han, J. Zhang, Y. Qiao, J. Yu, Investigation of platinum utilization and morphology in catalyst layer of polymer electrolyte fuel cells, 79 (1999) 75-81
17. J. Xie, F. Garzon, T. Zawodzinski, W. Smith, Journal of the Electrochemical Society, 151 (2004) A1084-A1093

18. M.S. Saha, A,F, Gulla, R.J. Allen, S. Mukerjee, High performance electrolyte fuel cells with ultra-low PT loading electrodes prepared by dual ion-beam assisted deposition, Elec. Acta 51 (2006) 4680-4692
19. S.H. Akella et al., Studies on structure property relations of efficient decal substrates for industrial grade membrane electrode assembly development in pemfc, Scientific Reports, 8 (2018) 1-10
20. S. Shahgaldi et al, Development of a low temperature decal transfer method for the fabrication of proton exchange membrane fuel cells, International Journal of Hydrogen Energy, 42 (2017) 11813-11822
21. Y.G. Chun, C.S. Kim, D.H. Peck, D.R. Shin, Performance of a polymer electrolyte membrane fuel cell with thin film catalyst electrodes, J. Power Sources, 71 (1998) 174-178
22. G. Bender, T.A. Zawodzinski, A.P. Saab, Fabrication of high precision PEFC membrane electrode assemblies, 124 (2003) 114-117
23. A. Jaworek, A.T. Sobcyzk, Electrospraying route to nanotechnology: An overview, Journal of Electrostatics, 66 (2008) 197-219
24. J. Zeleny, Instability of Electrified Liquid Surfaces, Physical Review, 10 (1917) 1-7
25. G. Taylor, Disintegration of water drops in an electric field, Proc. R. Soc. Math. Phys. Eng. Sci., 280 (1964) 383-397
26. G. Taylor, Electrically driven jets, Proc. R. Soc. Math. Phys. Eng. Sci., 313 (1969) 453-475

27. M. Cloupeau, B. Prunet-Foch, Electrohydrodynamic spraying functioning modes: a critical review, J. Aerosol Sci., 15 (1994) 1021-1036
28. L.A. Smith, S.J. Thompson, United States Department of Agriculture - Agricultural Research Service research in application technology for pest management, Pest Management Science, 59 (2003)
29. K.S. Im, M.C. Lai, S.J. Yoon, Spray characteristics on the Electrostatic Rotating Bell Applicator, KSME International Journal, 17 (2003) 2053-2065
30. Y. Ishida, K. Hakiai, A. baba, T. Asano, Electrostatic inkjet patterning using Si needle prepared by anodization, Japanese Journal of Applied Physics, 44 (2005) 5786-5790
31. Tang, K., & Gomez, A. (1996). Monodisperse electrosprays of low electric conductivity liquids in the cone-jet mode.Journal of Colloid and Interface Science,184 , 500–511
32. S. Martin et al., Effect of the collector voltage on the stability of the cone jet mode in electrohydrodynamic spraying, Journal of Aerosol Science, 46 (2012) 53-63
33. J.L. Castillo et al., Morphology and Nanostructure of Granular Materials Built from Nanoparticles, KONA Poweder and particle Journal, 31 (2014) 214-233
34. O. Baturina, G. Wnek, Characterization of Proton Exchange Membrane Fuel Cells with Catalyst Layers Obtained by Electrospraying, 8 (2005) A267-A269
35. R. Benitez, A.M. Chaparro, L. Daza, Electrochemical characterisation of Pt/C suspensions for the reduction of oxygen, 151 (2005) 2-10
36. R. Benitez, J. Soler, L. Daza, Novel method for preparation of PEMFC electrodes by the electrospray technique, 151 (2005) 108-113

37. A.M. Chaparro. M.A. Folgado, P. Ferreira-Aparicio, A.J. Martin, I. Alonso-Alvarez, L. Daza, 157 (2010) B993-B999
38. A.M. Chaparro, B. Gallardo, M.A. Folgado, A.J. Martin, L.Daza, PEMFC electrode preparation: Optimization of catalyst load and ionomer content, Catalysis Today, 143 (2009) 237-241
39. S. Martin, P.L. Garcia-Ybarra, J.L. Castillo, Electrospray deposition of catalyst layers with ultra-low Pt loadings for PEM fuel cell cathodes, 195 (2010) 2443-2449
40. S. Martin, P.L. Garcia-Ybarra, J.L. Castillo, High platinum utilization in ultra-low Pt loaded PEM fuel cell cathodes prepared by electrospraying, 35 (2010) 10446-10451
41. S. Martin, B. Martinez-Vazquez, P.L. Garcia-Ybarra, J.L. Castillo, Peak utilization of catalyst with ultra-low Pt loaded PEM fuel cell electrodes prepared by the electrospray method, 229 (2013) 179-184
42. [B. Martinez-Vazquez, D.G. Sanchez, J.L. Castillo, K.A. Friedrich, P.L. Garcia-Ybarra, Scaling-up and characterization of ultralow-loading MEAs made-up by electrospray, International Journal of Hydrogen Energy, 40 (2015) 5384-5389
43. A.M. Chaparro, M.A. Folgado, P. Ferreira-Aparicio, A.J. Martin, L. Alonso-Alvarez, L. Daza, Properties of Catalyst Layers for PEMFC Electrodes Prepared by Electrospray Deposition, Journal of The Electrochemical Society, 157 (2010) B993-B999

44. A. Fischer, J. Jindra, H. Wendt, Porosity and catalyst utilization of thin layer cathodes in air operated PEM-fuel cells, Journal of Applied Electrochemistry, 28 (1998) 277-282
45. D. Singh, D.M. Lu, N. Djilali, A two-dimensional analysis of mass transport in proton exchange membrane fuel cells, International Journal of Engineering Science, 37 (1999) 431-452
46. H. Tang, S. Wang S.P. Jiang, M. Pan, A comparitive study of CCM and hot-pressed MEAs for PEM fuel cells
47. J.H. Hirschenhofer, D.B. Stauffer, R.R. Engleman, M.G. Klett, Fuel Cell Handbook, fourth ed., Business/Technology Books, California, 1998
48. R. O'Hayre, S.W. Cha, W. Colella, F.B. Prinz, Fuel Cell Fundamentals, first ed., John Wiley & Sons, New York, 2006
49. J. Wu, X.Z. Yuan, H. Wang, M. Blanco, J.J. Martin, J. Zhang, Diagnostic tools in PEM fuel cell research: Part I Electrochemical techniques, International Journal of Hydrogen Energy, 33 (2008) 1735-1746
50. Experimental Methods and Data Analyses for Polymer Electrolyte Fuel Cells, ed. 1.17, Scribner Associates, Inc., South Pines, NC, USA
51. Fuel Cell Test Software for Scribner Associates Fuel Cell Test Systems, Version 4.2, Scribner Associates, Inc., South Pines, NC, USA
52. D. Ubeda et al., Life test of a high temperature PEM fuel cell prepared by electrospray, International Journal of Hydrogen Energy, 41 (2016) 20294-20304

53. U.A. Hasran et al., Optimization of hot pressing parametrs in membrane electrode assembly fabrication by response surface method, 38 (2013) 9484-9493